

# The ESO Faint Object Spectrograph and Camera (EFOSC)

B. Buzzoni, B. Delabre, H. Dekker, S. D'Odorico, D. Enard, P. Focardi, B. Gustafsson, W. Nees, J. Paureau and R. Reiss, ESO

## History

In the year 1981, the Instrumentation Group, then under the direction of D. Enard, started a design study for a Low Dispersion Spectrograph for the ESO 3.6 m telescope. In September 1982, a decision was taken for a Focal Reducer type instrument at the Cassegrain focus. Prestudies, including flexure analysis and optical design, were completed early in 1983. Integration tests started in Garching in the beginning of 1984; a first telescope test was performed successfully in June 1984.

H. Dekker was project manager. S. D'Odorico, who became Head of the Optical Instrumentation Group in 1983, provided the overall guidance in the integration and astronomical test phases. B. Delabre was responsible for the optical design. J. Paureau and G. Hess designed the mechanics and the structure and W. Nees and B. Gustafsson were responsible for electronics and control software. During the test phase, B. Buzzoni did the integration and R. Reiss installed and tuned the CCD. P. Focardi helped reducing and assessing the quality of the test observations.

The instrument will be available for general use in low dispersion spectroscopy and direct imaging modes from April 1985. Manuals are in preparation and will be available at this date (1), (2). Multiple object spectroscopy will probably be offered six months later.

## Design Options

The goal of the study was to find a very efficient instrument configuration with which low dispersion spectroscopy (down to 100 Å/mm) and field spectroscopy could be done. A

capability for direct imaging was thought to be essential, both for the acquisition of very faint objects and for photometry. It was intended to use a thin, back-illuminated RCA CCD with 512 x 320 pixels of 30 μm. Initial solutions were investigated based on concave gratings in the primary focus. However, it appeared that it is presently not yet possible to make efficient F/3 concave gratings, either holographic or ruled. Also, the prime focus is more difficult to access and offers rather limited space. An advantage is obviously the single reflection in the telescope.

For the Cassegrain, a simple, compact and very efficient configuration was found, consisting of a focal reducer, converting the F/8 telescope beam to F/2.5. A parallel beam space was foreseen in which grisms of filters can be inserted. This solution was finally adopted. Enard and Delabre discuss the different optical design options in more detail in (3).

## Design

As always in the design of an astronomical instrument, an important question to answer is the projected pixel size on the sky. As a compromise between the requirements for direct imaging and spectroscopy and taking into account the average seeing at the 3.6 m, we finally fixed the camera speed to F/2.5, giving a pixel size of .67" for the RCA chip we use.

The other key parameter is the camera focal length which determines the dispersion attainable with a given grism. Scaling the instrument up rapidly increases the complexity of optics and mechanics. A focal length of 100 mm provides dispersions of up to 120 Å/mm. (The active grating area is still only 40 mm in diameter which keeps grating costs down.)

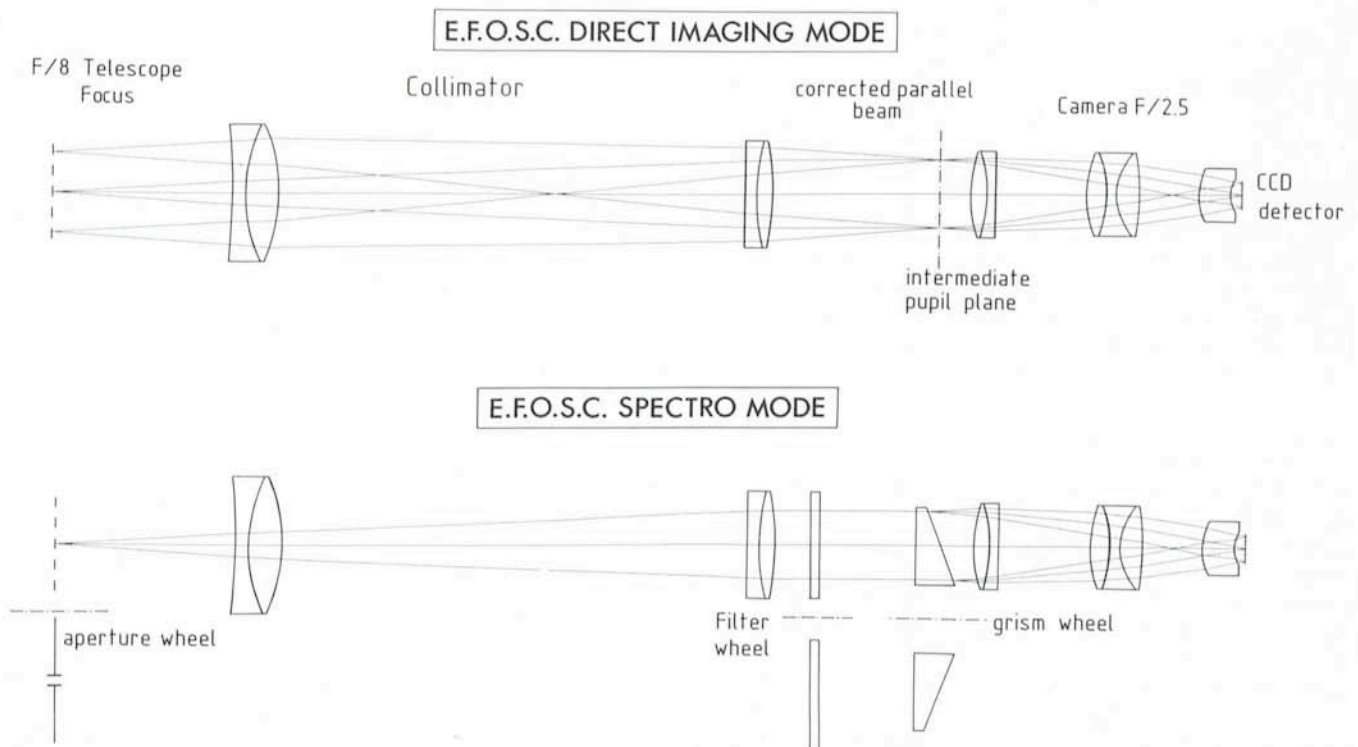


Fig. 1: The optical design of EFOSC.

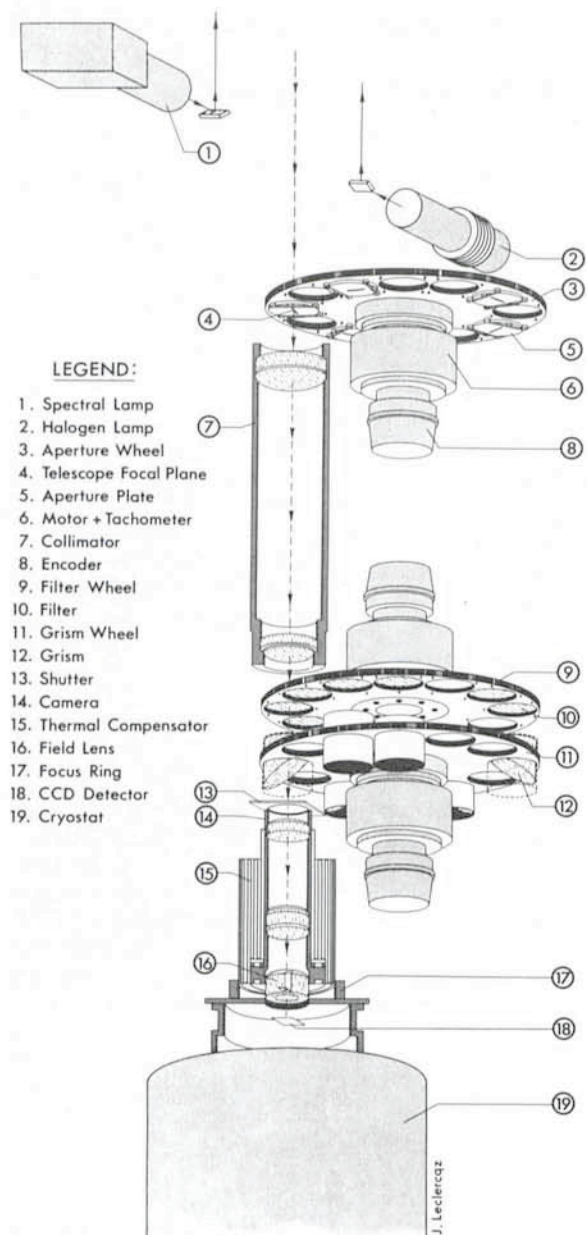


Fig. 2: EFOSC layout.

The focal reducer is totally based on lens combinations; it has no mirrors and presents no vignetting or central obscuration. Its main elements are a collimator, consisting of 2 lens groups, and a camera consisting of 3 lens groups (see Fig. 1). The collimator produces an image of the telescope entrance pupil just in front of the camera. The aspheric camera field lens also serves as a cryostat window. Up till now, fully dioptric spectrographs were rather unusual in astronomy, they are now conceivable because of new developments in glasses, optical design programmes, high-efficiency coatings and dispersing elements (grisms).

The image quality – characterized by the diameter which encircles 80 % of the geometrical energy – of this design is quite good; in white light (3500–10000 Å) imaging, the image quality in the central 10 mm of the field is better than .3", in the corners the quality is about .5". This result could only be reached by using a new glass (Schott type FK54) which allows excellent secondary colour correction, while at the same time its blue transmission is still quite acceptable, unusual for a glass of this type. It also has disadvantages, notably its very high coefficient of expansion (twice that of a normal glass) and local glass homogeneity problems (schlieren) which are how-

ever not a limiting factor for the relatively small lenses of EFOSC. The difference in thermal expansion coefficient requires care in the cementing of the lenses and in the handling.

A slight disadvantage of this type of design is the so-called sky concentration, also known from wide-field telescope correctors. It appears as a diffuse spot, 5–10 % above the background in the centre of the image. It is caused by light which is back-reflected by the chip into the camera and returned by some optical surface. Optically, it can be seen as the superposition of several demagnified out-of-focus images of the CCD, each image corresponding to an optical surface. The largest contributions come from the field lens. Our experience indicates that flat-fielding will correct this effect to better than 1 %.

Fig. 2 gives a view of the instrument. It is equipped with 3 wheels, each with 12 positions. Table 1 lists the currently available slits and filters. Note that all filters must have image quality over the full 50 mm used – an important consideration for users bringing their own filters. The grism wheel holds up to 9 grisms, providing different dispersions and wavelength coverage. Two positions are reserved for Hartmann screens, to be used for focusing.

The camera is mounted in a thermal compensator, a unit which automatically moves the camera lenses with temperature to maintain the focus. The user needs only to focus the telescope.

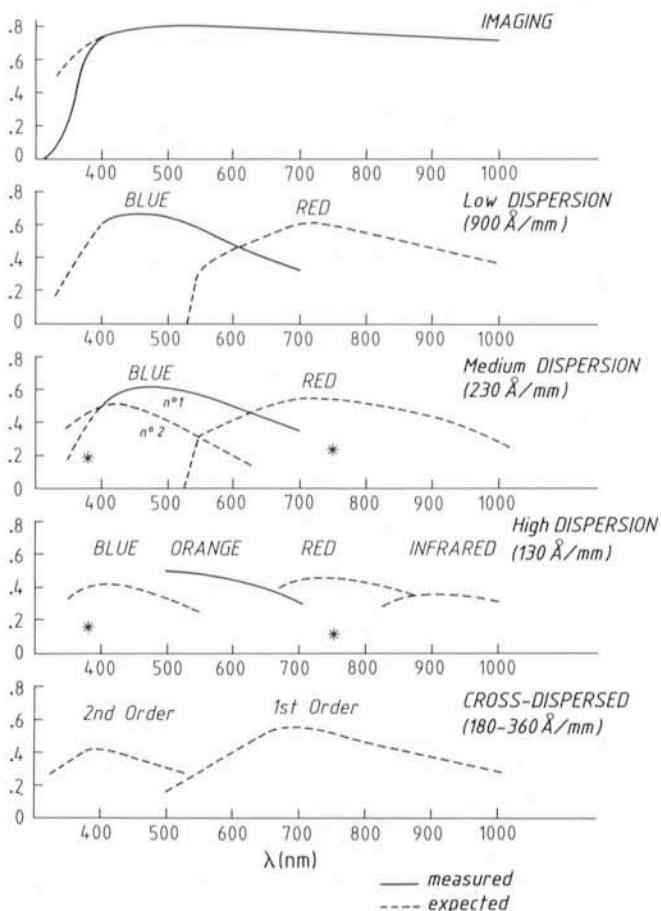


Fig. 3: Efficiency and wavelength coverage in imaging and spectroscopic modes. Full lines represent actual measurements, dotted lines are values expected for components which were not yet received. The lenses are being recemented because of problems with the UV transmission of the previously used cement. The stars represent the efficiency of the Boller and Chivens spectrograph at comparable dispersions.

Above the aperture wheel, four calibration lamps are mounted, one halogen and three spectral lamps.

The only useful coating available for the very large wavelength range is a quarter-wave MgF<sub>2</sub> layer, peaked at about 5000 Å. The average optical throughput between 3500 and 10000 Å is 75 %, with a maximum of 82 % at 5500 Å. In Fig. 3, the overall optical efficiency is shown in direct imaging and spectroscopic modes.

The structure was designed for high rigidity and is shaped as a box, closed on three sides. The fourth side is open for easy access. All units are pinned for reproducible mounting. Flanges at both ends attach to the telescope and to the CCD cryostat (see Fig. 4). Flexure tests (1) have shown that image movement is negligible (< 0.1 pixel) for a 30 degree attitude change, corresponding to an exposure time of 2 hours.

The 3 wheels are driven by direct-drive DC motors with the wheels, tacho and encoder mounted directly on the motor axis. This eliminates backlash which is always a problem when gearboxes are used. The encoders have a resolution of .001 degree; the absolute positioning accuracy of the servo loop is better than .005 degree. The HP 1000 computer sends its motor position command to microprocessor controlled CAMAC modules which provide the position and velocity servo control.

The software consists of three main programmes. With the user interface programme, softkey menus can be chosen and forms filled in; the instrument control programme takes care of the CAMAC communication and the CCD programme sends control commands to the detector and reads out and stores the images on disk. The user interface also provides access to the IHAP image processing programme. For more information about the software see [4].

## Operation and Maintenance

In EFOSC, a large number of filters and grisms with different dispersions can be mounted at the same time. This allows a high degree of flexibility in the scientific programmes which can be carried out. Switching from imaging to the spectroscopic mode is accomplished in a few seconds.

Pointing in the spectroscopic mode is done by inserting the mirror mounted in the aperture wheel and centring the object with the slit viewer. If it is too faint to be seen on the TV, a short exposure has to be taken. With an exposure of a few minutes it is possible to reach 23rd magnitude which is about the present limit for spectroscopy. From the image, the offsets to be given to the telescope to centre the object on the slit are computed with a standard batch programme.

Guiding in imaging and spectroscopic modes is done on an offset star. An auto-guider should also be available at the 3.6 m at the beginning of 1985.

The multiple object spectroscopy mode requires a CCD frame of the field to be taken to measure the positions of the objects to be observed. The following morning, an aperture plate is prepared in the La Silla workshop and mounted in the instrument. This procedure has been tested successfully in June and it will be illustrated in detail in a forthcoming article.

EFOSC is a very simple instrument, requiring little maintenance. From time to time, however, checks must be done on the alignment and position of the slits, of the grisms, etc. For this purpose, the instrument control programme can make a series of test exposures during daytime. The resulting images are subsequently automatically analyzed by an IHAP batch programme and the result printed out. A complete self-test sequence will last approximately 2 hours; the print-out documents the condition of the instrument and indicates if corrections must be applied.

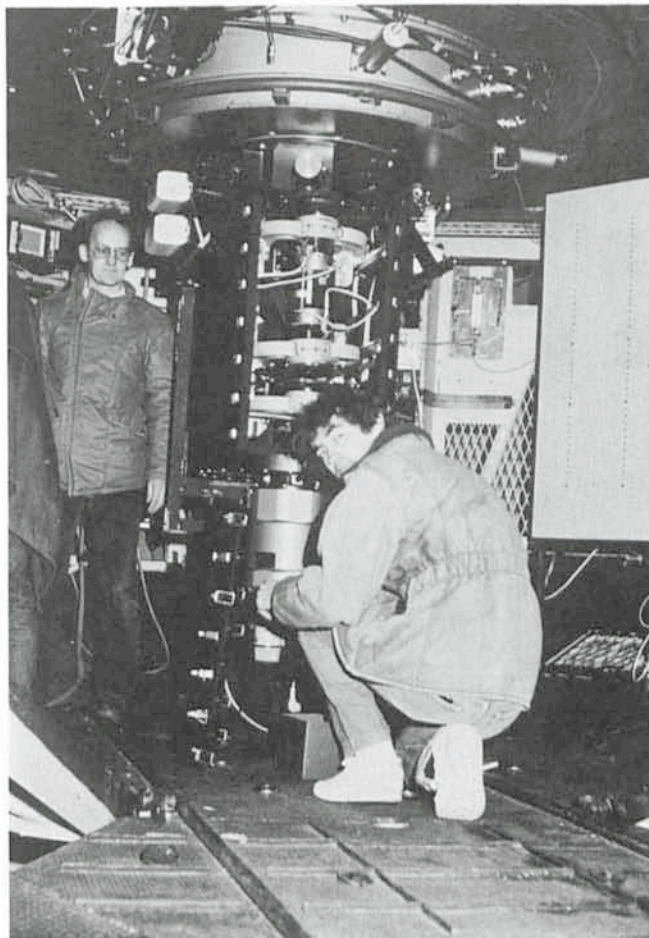


Fig. 4: The instrument on the telescope. A door in the light-tight enclosure has been removed to exchange filters. On the upper flange, calibration lamps and electronics box are mounted.

## First Results at the Telescope

During the test period at the 3.6 m telescope we checked the different modes of operation and the limiting performance of the instrument. The overall results were quite satisfactory even if the astronomical observations were restricted to two nights in bright moon time due to the poor weather.

An RCA back-illuminated CCD with 40 e rms read-out noise and a peak quantum efficiency of 80 % was used as a detector. The spectrograph, the control programme and the detector worked smoothly throughout the test period. Spectroscopic observations of two QSOs of 17th and 20th magnitude at 7 Å/pixel have already been published (5). From these we estimate the actual efficiency of the spectrograph and detector to be .47. The value predicted from the measured transmission of the optics and the detector characteristics is .50. At 7 Å/pixel and with the present detector the limiting magnitude is about 22 for a 90-minute exposure.

Because of the moon, we obtained only a few photometric data in the direct imaging mode. In the R band stars of 22 magnitude are well detected in a 3-minute exposure. The efficiency of EFOSC can also be judged from the deep view of the Kepler supernova remnant which is shown in Fig. 5.

Observers will also be interested in the flat-fielding and data reduction procedure. For the flat-fielding of the images and of the spectra and for wavelength calibration a reflecting screen was mounted on the top of the telescope sky baffle. Dimension and central obscuration match those of the primary mirror and

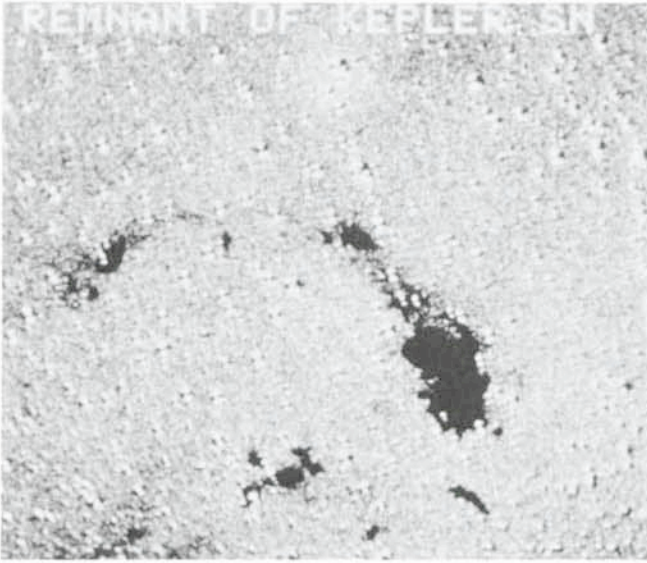


Fig. 5: A deep image of the remnant of the Kepler supernova (1604 AD) was obtained by subtracting a continuum exposure from one taken through a  $60 \text{ \AA}$  interferential filter centred at  $6562 \text{ \AA}$ . Exposure times were 15 minutes. It is the first time that the optical shell, which has well defined radio and optical counterparts, is seen so clearly.

it can be inserted remotely in the optical path to reflect the light from the calibration lamps. The calibration procedure is very rapid and it works very well for the spectra. In direct imaging the results are satisfactory (see Fig. 6).

As for data reduction, images are obviously in the same format as e. g. the CCD data with the 2.2 m direct camera with which many ESO observers are familiar. They can be reduced at ESO Garching either with the IHAP or MIDAS systems. The spectra with the standard apertures are in the same format as data from the Boller and Chivens + CCD. They can be fully reduced with IHAP. Some further software development is required for the analysis of "direct" grism images and for multiaperture spectroscopy.

## Conclusions

From the first tests at the telescope, EFOSC proved to be a valuable and docile instrument. It is not only the most efficient ESO low dispersion spectrograph but – we like to think – one of the best worldwide in its category. It has a versatile deep imaging capability. We certainly hope it will produce a lot of good data for those programmes which require observations of faint objects.

## A Word of Thanks

As is evident from the list of authors, a large team contributed to the development of this instrument in Garching. We want to express our thanks to the staff in La Silla for their excellent assistance during the installation and test on the telescope. A particular thanks goes to L. Baudet and G. Ihle.

## References

- (1) EFOSC Technical Report, in preparation.
- (2) EFOSC Operating Manual, in preparation.
- (3) D. Enard, B. Delabre, 1982, Two design approaches for high efficiency, low resolution spectroscopy. Proceedings SPIE **445**, 522.

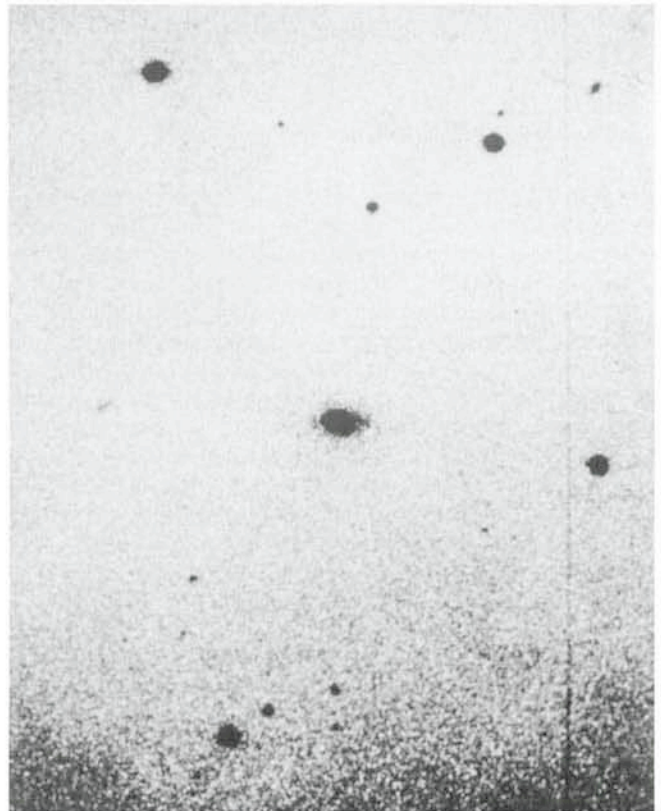
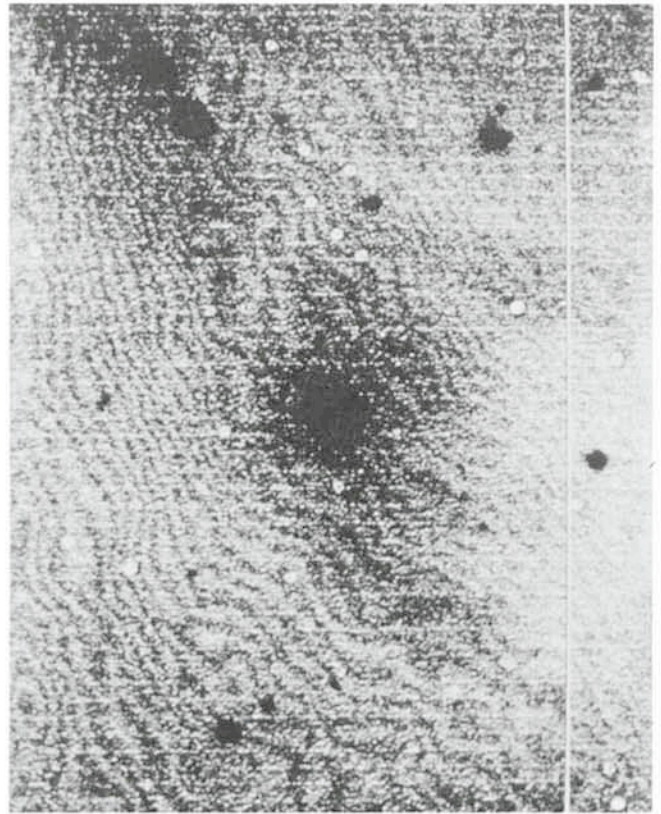


Fig. 6: (a) An EFOSC 15-minute exposure of the radio galaxy PKS 2158-380 through a  $60 \text{ \AA}$  wide interferential filter centred at  $5007 \text{ \AA}$ . The peak-to-peak intensity of the fringes is at most 5%. The "sky concentration" at the centre has about the same intensity. (b) The same image after division by the flat field obtained by illumination of a screen inserted in the optical path of the telescope with a calibration lamp. Fringes and sky concentration are corrected to better than 2%. A uniform gradient of amplitude 5% is introduced at one edge of the image by the flat-field image which is not fully uniform. While this effect does not prevent accurate photometry to be done, we hope to eliminate it by modifying the lamp support.

- (4) P. Biereichel, B. Gustafsson, G. Raffi, 1983, The New Data Acquisition System for ESO Instrumentation, *The Messenger* **34**, 35.
- (5) H. Dekker and S. D'Odorico, 1984, First QSO Spectra with EFOSC, *The Messenger* **37**, 7.

Table 1. Available filters and standard apertures.

In the filter wheel, up to 11 filters may be mounted. The aperture wheel will hold up to 10 standard or special (multi-hole) aperture plates; one position is reserved for an inclined mirror for use with the slit viewer, one position must be free for direct imaging. The twin slits are primarily intended to be used with the cross-dispersed grism.

#### Filters

A set of redshifted H $\alpha$  and [OIII] interference filters:

Redshift	Centre wavelength/FWHM	
km/sec	[OIII]	H $\alpha$
0	5010/66/130	6562/61/142
3000	5060/56	6634/70
6000	5111/55	6693/94
9000	5162/63	6766/68
12000	5211/60	6832/74
15000	5261/54	
18000	5313/55	6956/64
21000	5354/64	7018/64

A set of U, B, V, R filters.

A set of Gunn G, R, I, Z filters.

#### Standard aperture plates:

Slits with a length of 3.6':  
.5", .75", 1", 1.5", 2", 2.5", 3", 5", 10".

Twin slits 50" apart, each 5" long:  
1", 1.5", 2", 3", 6".

## Abundances in LINERs

L. Binette, ESO

### Introduction

Ionized gas can be detected in the nucleus of most bright galaxies as shown by the recent surveys of Keel (1), Stauffer (2), Phillips et al. (3) and Heckman et al. (4). In fact, Keel detected nuclear emission in all the spiral galaxies (not edge-on) of his magnitude-limited complete sample. Apart from demonstrating that nuclear emission is a common phenomenon, these surveys also showed that the emission can be broadly divided into three classes: those that bear many similarities with spiral arm HII regions and for which young OB type stars are the likely excitation mechanism; secondly, those that are characterized by low excitation lines such as [NII], [OII], [SII] and [OI], which have been termed LINERs (for Low Ionization Nuclear Emission Regions) by Heckman (5), and, finally, the higher excitation (and rarer) Seyferts galaxies which often reveal an important UV continuum excess. The recognized excitation mechanism for Seyferts is photoionization by a non-stellar object.

In the case of LINERs, the excitation mechanism is still debatable. Because of the predominance of low ionization species in the spectra, excitation by shocks appeared promising at first and has been proposed by Heckman. However,

recent work by Ferland and Netzer (6), Halpern and Steiner (7) and Keel (8) shows that photoionization by non-thermal UV spectra more easily reproduces the spectral features of LINERs; the latter are also shown to form a natural sequence with Seyferts or Quasars with the ionization parameter as the connecting variable. In support of this, properties like broad Balmer lines or nuclear X-ray flux which are often associated with Seyferts, are also observed in a substantial fraction of LINERs. Although photoionization is adopted in the analysis that follows, the possibility that both mechanisms may be operating to different degrees in different objects cannot be ruled out (Aldrovandi and Contini (9)).

We here present a project summary on LINERs for which two types of results are available at this stage: first, new diagrams of emission line ratios which reveal tighter correlations when homogeneous data are used, second, a new grid of photoionization calculations which aim at analysing the sensitivity to input parameters like optical thickness, hardness of the ionizing spectrum and distribution of the gas. It is concluded that abundances are more uniform (and solar) than previous work suggested.

### New Diagnostic Diagrams for LINERs

Although photoionization models have proved successful in reproducing various correlations in selected diagnostic diagrams, the scatter of the data remained nevertheless substantial. From trying out new combinations of line ratios, however, it has become apparent that this scatter can be significantly reduced if one defines diagrams which are optimized for the type of spectrum that characterises LINERs; as a by-product, these new diagrams also give more compelling evidence in favour of photoionization. For example, there are many advantages in replacing the much in vogue OII/OIII axis which represents the excitation of the gas, by OI/OIII, an equivalent excitation index. (Obviously, this is only possible for classes of objects like LINERs which present a significant [OI] flux). While the previously used OIII/H $\beta$  versus OII/OIII diagram is significantly affected by interstellar extinction or by collisional deexcitation due to high densities, the new diagram proposed in Fig. 1 is quite insensitive to these effects. In fact, the dispersion introduced in Figs. 1 and 2 due to reddening is quite small because the reddening correction (represented by the arrow normalized to E(B-V) = 0.66) runs in about the same direction as the correlation shown by the objects. Similar considerations apply to the effect on the line ratios of collisional deexcitation. For instance, the dispersion introduced by varying the densities is no more than 0.24 dex if these are below  $4.0 \times 10^5 \text{ cm}^{-3}$  (this result is born out of computations of models such as those described below). Another factor favouring Fig. 1 is that it is quite insensitive to geometrical parameters defining the gas distribution as has been shown using spatially "integrated" models. Unfortunately, one parameter – optical thickness – could pose a serious problem for any diagram involving [OI] but, as it turns out, the ionized condensations appear to be optically thick at least in the majority of the objects. This is indicated by the scatter which should otherwise be larger than observed in Fig. 1. The possibility of optical thinness is further discussed in Binette (10).

A set of spectral data on LINERs larger than available to Ferland and Netzer or Halpern and Steiner is plotted in Figs. 1 and 2; it includes data from both Keel (8) and Stauffer (11). (A few ellipticals have been added by Keel to the subset). These data are represented by squares except for the higher excitation objects of Stauffer for which diamonds are used. These latter objects would not strictly be classified as LINERs if Heckman's criterion concerning the relative strength of [OIII] is